Chin. J. Astron. Astrophys. Vol. 7 (2007), No. 4, 457–476
(*http://www.chjaa.org*)

Chinese Journal of
Astronomy and
Astrophysics

Observational Features of Large-Scale Structures as Revealed by the Catastrophe Model of Solar Eruptions *

Jun Lin

National Astronomical Observatories / Yunnan Observatory, Chinese Academy of Sciences, Kunming 650011; *jlin@ynao.ac.cn*
Harvard-Smithsonian Center for Astrophysics, 60 Garden Street, Cambridge, MA 02138, USA

Received 2006 October 15; accepted 2007 April 23

Abstract Large-scale magnetic structures are the main carrier of major eruptions in the solar atmosphere. These structures are rooted in the photosphere and are driven by the unceasing motion of the photospheric material through a series of equilibrium configurations. The motion brings energy into the coronal magnetic field until the system ceases to be in equilibrium. The catastrophe theory for solar eruptions indicates that loss of mechanical equilibrium constitutes the main trigger mechanism of major eruptions, usually shown up as solar flares, eruptive prominences, and coronal mass ejections (CMEs). Magnetic reconnection which takes place at the very beginning of the eruption as a result of plasma instabilities/turbulence inside the current sheet, converts magnetic energy into heating and kinetic energy that are responsible for solar flares, and for accelerating both plasma ejecta (flows and CMEs) and energetic particles. Various manifestations are thus related to one another, and the physics behind these relationships is catastrophe and magnetic reconnection. This work reports on recent progress in both theoretical research and observations on eruptive phenomena showing the above manifestations. We start by displaying the properties of large-scale structures in the corona and the related magnetic fields prior to an eruption, and show various morphological features of the disrupting magnetic fields. Then, in the framework of the catastrophe theory, we look into the physics behind those features investigated in a succession of previous works, and discuss the approaches they used.

Key words: Sun: large-scale magnetic structures — Sun: eruptive processes — Sun: theory and observations — magnetic reconnection and current sheets

1 INTRODUCTION

The large-scale structures related to eruptive phenomena in the solar atmosphere can be classified into two categories: (quasi-)static structures in equilibrium and dynamic structures in eruption. The former usually appears in the form of solar filaments, and the latter mainly in the form of solar flares and the associated manifestations, such as eruptive prominences and coronal mass ejections (CMEs).

Solar filaments (also know as prominences) are cool dense plasma embedded in the hot tenuous corona. They are located at the polarity inversion lines (PILs) that separate regions of opposite magnetic polarities in the photosphere, and are presumably supported by the coronal magnetic field (Kiepenheuer 1953). In response to slow mass motions in the photosphere where the filament is rooted, the filament and the related magnetic field evolve continuously. Initially, the evolution is smooth, then, the stress, together with the free energy (the difference between the magnetic energies of the stressed, or non-potential, and the

* Supported by the National Natural Science Foundation of China.

corresponding potential systems), gradually builds up in the coronal magnetic field. When the free energy exceeds a threshold (or critical value), the evolution turns into a dynamic one with a rapid release of the free energy. All filaments eventually erupt no matter whether they are initially quiescent or active (e.g., Tandberg-Hanssen 1974; Švestka 1976; Priest 1982). The dynamical evolution shows much richer manifestations than the quasi-static evolution, the three main ones being solar flare, eruptive prominence and CME while separating flare ribbons on the solar disk and growing flare loops in the corona constitute the most significant features of the eruptions near the solar surface.

In the framework of the catastrophe model, the filament is usually modeled by a flux rope carrying electrical current (e.g, Lin & Forbes 2000). The helical structure inside the flux rope produces magnetic compression which pushes the flux rope upward as a result of interaction between the current associated with the helical structure and the background field (e.g., Forbes & Isenberg 1991). The model assumes a geometry whereby the prominence, the flux rope, and the CME core are co-located. This is done for mathematical convenience although in some observed CMEs these structures do seem to be co-located. Equilibrium in the magnetic configuration is realized as the magnetic compression and tension forces acting on the flux rope balance each other. The magnetic tension is in the field lines passing over the top of the flux rope and anchored in the photosphere. Catastrophe occurs and the flux rope is thrust outward when the tension fails to balance the compression.

Models also exist where helical structures were not present in the initial magnetic field, rather, they are produced by magnetic reconnection in the corona during the eruption (Mikić & Linker 1994; Antiochos et al. 1999). Due to the lack of helical structure, there is no magnetic compression, and magnetic reconnection in the coronal fields is necessary to trigger the loss of equilibrium in the system prior to the eruption, in contrast to the catastrophe model in which the loss of equilibrium is a purely ideal-MHD process (e.g., Forbes & Isenberg 1991). In fact, the flux rope and non-flux rope models are less distinct than is generally thought. The only difference is that the reconnection producing the flux rope occurs in the photosphere in the flux rope model (e.g., MacKay & van Ballegooijen 2005) and in the corona in the non-flux rope model. As the eruption proceeds, the two models do not manifest any significantly different observational consequences (e.g., Linker et al. 2003; Lin et al.2004; Lynch et al. 2004; MacNeice et al. 2004). Some non-flux rope models did not show features of current sheets (MacNeice et al. 2004; Lynch et al. 2004) because of insufficient resolution of the grid in the numerical code used in the simulations. In the present work, we focus on the flux rope model and its observational consequences. We start with various aspects of magnetic fields prior to the eruption in next section, and discuss the newly emerging magnetic flux and its role in triggering eruptions in Section 3. We unfold the morphological features of the disrupting structure in the course of the eruption in Section 4. Various aspects related to the reconnecting current sheets developed in the eruptions will be discussed in Section 5, and the correlations between CMEs and other activities, in Section 6. In Section 7 the start frequency and the onset position of type II radio bursts induced by the CME-driven shocks will be investigated on the basis of our previous works. We summarize this work in Section 8.

2 LARGE-SCALE STRUCTURES PRIOR TO ERUPTION

Prior to the eruption, objects obviously connected to the large-scale organizations are the filament (or prominence) and the related magnetic structures. Filaments are formed in "channels" where the chromospheric fibrils are aligned with the PIL (Foukal 1971; Martin 1990; Gaizauskas et al. 1997). This alignment indicates the presence of a horizontal "axial" magnetic field directed along the length of the channel. In the northern (southern) hemisphere of the Sun, the direction of the axial field is predominantly to the right (left) when viewed from the positive polarity side of the filament channel (Martin et al. 1994). In addition to the axial field, there may also be a "poloidal" component, together forming a weakly twisted helical flux rope with the filament plasma located at the dips of the helical windings (e.g., Kuperus & Raadu 1974; Priest et al. 1989).

Some filaments are formed in simple bipolar regions in the way shown in Figure 1 (from van Ballegooijen & Martens 1989): an initial potential field becomes sheared and non-potential due to motions at the footpoints along the PIL (Fig. 1a), converging motions toward the PIL further enhance the magnetic shear and cause magnetic reconnection (or cancellation) to occur at the footpoints, producing a helical structure in the system (Fig. 1b). Continuous shearing motion and reconnection successively transport magnetic

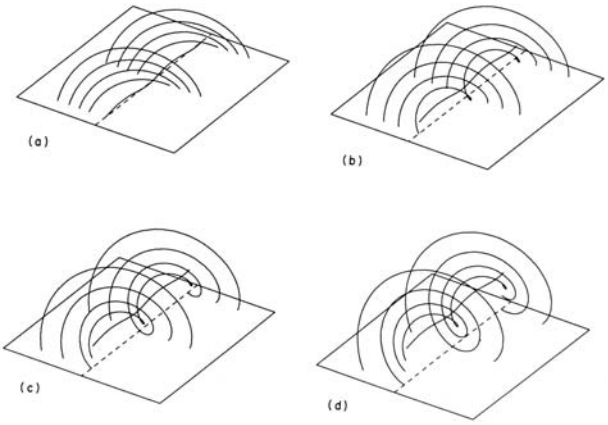

Fig. 1 Schematic description of filament formation in a simple bipolar region: (a) plasma flow at the footpoints along the PIL produces sheared magnetic field; (b) field lines become closed due to magnetic cancellation occurring at the PIL as the footpoints are pushed towards the PIL by converging flows; (c) existence of the helical structure allows the prominence material to float in the corona; (d) further evolution in the system pushes the prominence to higher altitudes until equilibrium breaks down, from van Ballegooijen & Martens (1989).

flux and plasma into the corona, allowing the prominence material to float in the corona (Fig. 1c), and further evolution in this way accumulates more free energy in the system and pushes the prominence toward the critical altitude where the eruption occurs (Fig. 1d). These four panels illustrate how magnetic cancellation in a sheared arcade leads to the formation of a prominence with helical field lines, and an increase in the height of the prominence. The role of magnetic flux cancellation in the evolution of the coronal magnetic field and in triggering eruptions has been well recognized since the process was reported and started to be investigated in detail two decades ago (e.g., Livi et al. 1985; Wang et al. 1988; Wang et al. 1996; Zhang et al. 2001a; Contarino et al. 2006, and references therein).

Generally, eruptions occurring in a simple bipolar system as shown in Figure 1 often develop a pair of roughly parallel flare ribbons along either side of the PIL on the surface. In this situation, the flare ribbons move almost perpendicularly to their length and to the PIL. This makes it very easy and straightforward for us to investigate the physical properties of the magnetic reconnection in progress in the current sheet via analyzing the motions of the flare ribbons and loops. Examples of such events can be found in the previous works by Švestka (1976), Moore et al. (1980), Poletto & Kopp (1982), Wang et al. (2003) and Qiu et al. (2004).

The majority of filaments are formed at the borders of active regions or in between active regions (Tang 1987). For example, Gaizauskas et al. (1997) described the formation of a channel between a compact active region and an older, more dispersed region. This suggests that the multipolar structure of the coronal field plays an important role in the formation of the filament channel. One such example was described by Liu et al. (2003), in which a prominence appeared between two active regions and eventually erupted ejecting a helical flux rope and producing a two-ribbon flare (X-3 class).

The corresponding scenario of flux rope formation between two active regions is illustrated in Figure 2 (from Lin & van Ballegooijen 2005). When two active regions emerge into the solar atmosphere, they initially form two separate flux systems (Fig. 2a). Soon afterward, magnetic reconnection occurs between them (Priest & Raadu 1975), forming a quadrupolar configuration containing an X-type neutral point in the corona between the two regions (Fig. 2b). Evidence for such reconnection may be found in X-ray loops connecting different active regions within a few days after the birth of a new region (Sheeley et al. 1975; Chase et al. 1976; Švestka et al. 1977; Tsuneta 1996).

Subsequently, the magnetic field evolves in response to the solar differential rotation and supergranular flows, causing the dispersal and decay of the active regions on time scales from days to months (Leighton

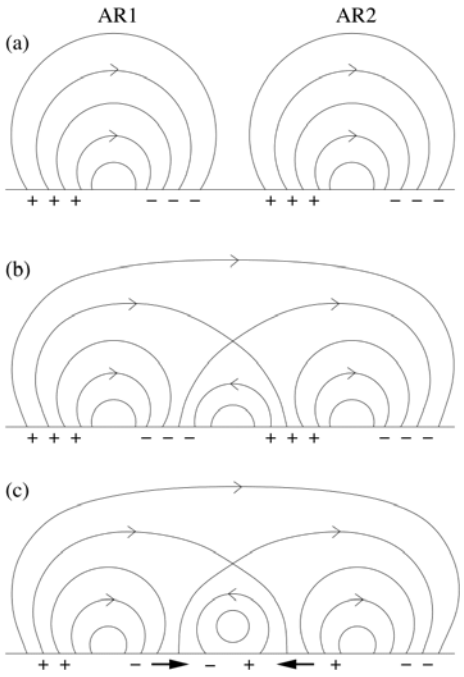

Fig. 2 Schematic description of the interaction between two active regions, and of the formation of a flux rope: (a) Two active regions commence to appear in the solar atmosphere, (b) communication between them is built up forming an X-type neutral point in the corona, and (c) magnetic reconnections occur in both the corona (at the X-point) and the photosphere (at the PIL), together with various types of photospheric motions, creating a current-carrying flux rope (filament) in the corona, from Lin & van Ballegooijen (2005).

1964; Wang et al. 1989; Schrijver & DeRosa 2003). In this process opposite polarity fluxes cancel each other at the three PILs (two inside and one in between the active regions). This has major effects on the overlying coronal field: as the photospheric footpoints disappear, the coronal field lines must reconnect, especially where the magnetic field is strongly sheared along the PIL (van Ballegooijen & Martens 1989). The second type of reconnection occurs at the PILs and produces flux ropes just above each PIL (see Fig. 2c; only the cross-section of the central flux rope is shown). Flux rope formation is also found to occur in the numerical experiments (e.g., MacKay & van Ballegooijen 2005), but the early codes are not suitable for studying the further evolution of the system that eventually turns into eruptions when the filament reaches the critical height. With recent improvement to the existing codes of the filament evolution it is now possible to continuously trace the formation and eruption of the filament (e.g., MacKay & van Ballegooijen 2006a,b).

It is also important to note that the magnetic configurations investigated by Lin & van Ballegooijen (2005) are similar to those in the breakout model of CMEs (e.g., Antiochos et al. 1999; Lynch et al. 2004; MacNeice et al. 2004), in that they have an X-point lying over a central arcade. They differ in that, in the catastrophe model, the central arcade always contains a flux rope, whereas in the breakout model such a flux rope does not appear until shortly after the eruption. Another significant point of the work of Lin & van Ballegooijen (2005) is that the evolution in the magnetic field shows apparently a catastrophic behavior which is not shown in the breakout model, although the magnetic fields have similar features. The difference results from the existence of a current-carrying flux rope and an associated helical field prior to the eruption.

Many researchers favor the idea that CMEs originate from helical coronal magnetic field with the form of a weakly twisted flux rope (see Low 1996 and 2001 for a review). Realistic three dimensional models of prominences based on flux ropes strongly support the existence of a flux rope prior to the onset of a CME (Aulanier et al. 2000), and the susceptibility of flux rope to ideal MHD instabilities (especially the kink instability) provides a natural explanation of why they might erupt (Hood et al. 1990; Sturrock et al. 2001).

In fact, after having carefully analyzed the properties of the magnetic configurations in both the sheared arcade model (e.g., Mikić et al. 1988; Mikić & Linker 1994; Linker et al. 2003) and the breakout model, we realized that the loss of equilibrium and thus the eruption in the system does not occur until a reconnection between the two legs of the sheared arcade is effected, although the reconnection between the arcade field and the overlying field in the breakout model has continued from the very beginning (e.g., Antiochos et al. 1999). The works by van Ballegooijen & Martens (1989), Amari et al. (2003), and MacKay & van Ballegooijen (2005) seem to indicate that, for the system to lose equilibrium a helical structure in the coronal magnetic field has to be created, no matter whether it is produced by reconnection in the corona or in the photosphere. In other words, a helical configuration in the corona is an intrinsic necessity for a major eruption.

3 NEW EMERGING MAGNETIC FLUX AND EVOLUTION IN THE CORONAL MAGNETIC FIELD

In the 1970s, new emerging flux was considered as possibly the main trigger of solar flares and perhaps also CMEs (Rust et al. 1980). Some ground-based observations appeared to show a strong correlation between solar flares and the emergence of new magnetic flux (Rust 1972, 1975). Rust (1972) and his coworkers (Rust & Roy 1974; Rust et al. 1975; Rust & Bridge 1975) found that flares sometimes occur close to rapidly evolving magnetic features which emerge with the opposite polarity to the surrounding region (Rust 1973). Their results also agree with the observations in Hα made by Vorpahl (1973). Motivated by these observations, Heyvaerts et al. (1977) proposed a plausible model of solar flares, which has subsequently received a great deal of attention. In this model a flare originates from the sudden onset of magnetic reconnection between newly emerging flux and an old preexisting flux system. The sudden onset is attributed to the appearance of a plasma microinstability within the current sheet which greatly enhances the effective resistivity, but the exact nature of the microinstability is not prescribed. One may find more information about these earlier observations and models in the reviews by Švestka (1976, 1981), van Hoven et al. (1980), Sturrock (1980), and Zirin (1988).

Martin et al. (1982, 1984) showed that the apparent correlation between emerging flux and flares was not sufficiently strong to support the model of Heyvaerts et al. (1977). Their studies seemed to suggest that something more than the onset of reconnection in a simple current sheet must be involved; thus the general interest in the emerging flux as a flare trigger waned. However, interest in emerging flux revived a decade ago when Feynman & Martin (1995) presented new observational evidence that eruptions of quiescent prominences and associated CMEs sometimes occur as a consequence of interaction between newly emerging active regions and the preexisting large-scale magnetic field containing the prominence. After analyzing more than 30 events they observed that prominence eruptions often occur shortly after the appearance of a new magnetic bipole in the vicinity of the prominence's magnetic channel. They also found that the orientation of the bipole relative to the magnetic channel was not important if the bipole emerged within the channel, close to the PIL, but that the orientation was important when the bipolar emerged outside the channel while still in the vicinity of the prominence. For these latter cases they found an orientation that permits an X-line to form in the corona between the emerging bipole and the prominence (i.e., an orientation defined as favorable for reconnection) would usually lead to an eruption, while an orientation which did not permit an X-line to form (i.e., the orientation defined as unfavorable for reconnection) would usually not lead to an eruption. However, not all of the studied events fit this pattern as there were a few exceptions which showed that sometimes eruptions occurred without the presence of a nearby newly emerging flux and that sometimes no eruption occurred despite the presence of newly emerging flux. Also there were a few cases where eruption occurred even though the orientation was unfavorable and a few which failed to erupt even though the orientation was favorable.

Later, Wang & Sheeley (1999) reported three examples of filament eruptions near new forming bipolar magnetic regions which support the findings of Feynman & Martin (1995). Several follow-up studies on the general properties of emerging flux in the photosphere have been completed by Canfield et al. (1996), Kurokawa & Santo (2000), Srivastava et al. (2000), Tang et al. (2000) and Chen & Shibata (2000).

Using a simple model for the onset of solar eruptions, Lin et al. (2001) investigated how an existing magnetic configuration containing a flux rope evolves in response to new emerging flux. Their results showed that the emergence of new flux can cause a loss of ideal MHD equilibrium under certain circum-

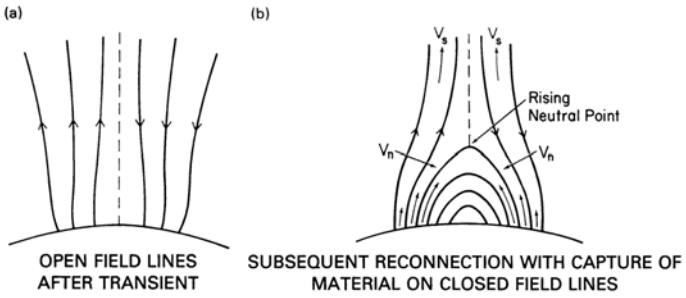

Fig. 3 Traditional Kopp-Pneuman model of two-ribbon flares: (a) the magnetic field is pushed open by an eruption and a current sheet separates two anti-parallel magnetic field lines, and (b) the opened configuration relaxes into a closed one via magnetic reconnection in the current sheet, from Kopp & Pneuman (1976).

stances, but the circumstances which lead to eruption are much richer and more complicated than one might expect from the given simple model. The results of the model suggested that the actual circumstances leading to an eruption are sensitive not only to the polarity of the emerging region, but also to several other parameters, such as the strength, distance and area of the emerging region. Therefore, despite the apparent simplicity of their two-dimensional model, it actually leads to a quite complex behavior, so much so, that it is difficult to extract any simple rule for predicting what types of emerging flux will produce an eruption.

Thus, the simple picture that new flux with an orientation favorable for reconnection will trigger an eruption by the cutting of the field lines overlying the flux rope is insufficient to describe the behavior Lin et al. (2001) observed. In hindsight this does not seem particularly surprising within the context of a flux rope model based on a loss of ideal MHD equilibrium. The occurrence of catastrophic behavior in such a model is not simply caused by a decrease of the magnetic tension that holds the flux rope in place or by an increase of the magnetic compression that pushes it upward. Normally, as one of the two forces is decreased or increased, the other automatically compensates so that equilibrium is maintained and no catastrophe occurs. It is only at special locations (i.e., the critical points of the equilibrium curves) that the forces cease to balance and catastrophe occurs. Lin et al. (2001) realized that reconnection between the new and old flux systems does not always drive the system to one of these critical points. Instead Lin et al. (2001) was only able to replicate the results of Feynman & Martin (1995) after carefully choosing the manner in which the new flux emerges, for example, by decreasing the depth of the emerging flux source while keeping its strength constant. Thus the fact that the behavior observed by Feynman & Martin (1995) is simpler than the model allows might be because of the way new flux emerges on the Sun. A realistic three-dimensional model is necessary to test this possibility.

4 MORPHOLOGICAL FEATURES OF MAGNETIC CONFIGURATIONS IN ERUPTIVE PROCESSES

In a major eruption, bright separating flare ribbons on the disk and growing flare loops in the corona clearly track the large-scale organizations near the surface. The motions of the flare ribbons and loops reflect the propagations of the energy release site through the magnetic configurations (Priest & Forbes 2002), and the pattern of motion of the flare loops is basically determined by the rate of magnetic reconnection in the current sheet which is controlled by the local Alfvén speed (Lin & Forbes 2000; Lin 2002), and that of the flare ribbons is governed by both the reconnection rate and the magnetic field distribution of the solar surface (Lin et al. 2004; Lin 2004a).

4.1 Formation of the Kopp-Pneuman Configuration

Kopp & Pneuman (1976) proposed a model of major (two-ribbon) flares (Fig. 3 from an idea first voiced by Carmichael in 1964 . See Švestka & Cliver 1992 for more details). In this model, energy is stored in a closed force-free magnetic arcade prior to the eruption. Eventually, the field erupts outwards to form a fully opened magnetic configuration including a neutral current sheet that separates magnetic fields of opposite

polarities (Fig. 3a). Then, the opened field lines continue to relax into the original state via reconnection in the sheet (Fig. 3b). The observational consequences of this process are two bright and separating flare ribbons on the solar disk, and a continually growing flare loop system in the corona. The motions of the flare ribbons and loops are not due to mass motions of the plasma but to the continuous erosion of the sheet and the associated upward propagation of the energy source to higher altitudes (Schmieder et al. 1987).

Recent works indicate that the closed magnetic field does not necessarily become fully open as in the Kopp-Pneuman-type eruption, instead, the closed magnetic structure is highly stretched by the eruption, producing a current sheet (Lin & Forbes 2000; Lin 2002; Lin et al. 2004; Chen et al. 2006). Both numerical simulations and analytical studies show that when the footpoints of a closed magnetic structure are sheared (Mikić & Linker 1994; Antiochos et al. 1999; Hu 2004; MacNeice et al. 2004), or when the whole structure is stretched outward by a catastrophic loss of equilibrium in a magnetic flux rope (Forbes & Isenberg 1991;Isenberg et al. 1993; Forbes & Priest 1995; Zhang et al. 2005, 2006), a current sheet develops in the stretched configuration. With dissipation in the current sheet, the stretched magnetic field lines start to reconnect through the sheet, restoring the original closed state before the upper part of the structure goes to infinity (Fig. 4), so that the pre-existing closed magnetic field does not necessarily become fully opened.

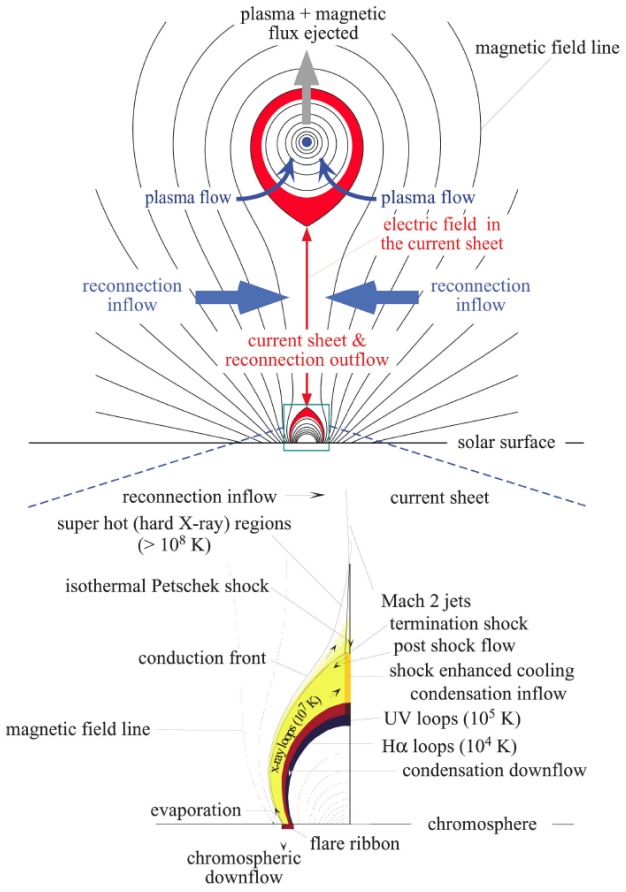

Fig. 4 Schematic diagram of a disrupted magnetic field that forms in an eruptive process. Colors are used to roughly indicate plasma layers of different temperatures. This diagram incorporates the two-ribbon flare configuration of Forbes & Acton (1996) and the CME configuration of Lin & Forbes (2000). More discussions about the CME part can be found in Lin et al. (2004).

4.2 Role of Magnetic Reconnection in the Eruption

The scenario sketched by Figure 4 suggests that reconnection plays a multiple role in an eruption. First, reconnection breaks the magnetic field lines that pass over the flux rope and anchored in the photosphere at both ends, and weakens the magnetic tension that prevents the flux rope from escaping. Second, reconnection dumps large amount of energy in the lower atmosphere, generating intensive heating, which accounts for the traditional flare ribbons and loops. Furthermore, the non-ideal MHD property of magnetic reconnection through the sheet helps resolving the so-called Aly-Sturrock Paradox (e.g., Aly 1991; Sturrock 1991; Forbes 2000; Lin et al. 2003), the difficulty of opening up the closed magnetic field lines via a purely ideal-MHD process occurring in the force-free configuration.

One of the most significant results in the Lin & Forbes (2000) model is that a current sheet develops following the onset of the eruption. Because the time-scale of reconnection is long compared to the time-scale of the onset stage (Alfvén time-scale), dissipation of the sheet by reconnection is slow, so, the sheet is able to become fairly long. Evolution of the sheet depends in a significant way on the local Alfvén speed. In an isothermal corona, the local Alfvén speed increases with height at large altitudes, so the sheet can be quickly eroded by reconnection and its length consequently shrinks a couple of hours after the onset (Lin & Forbes 2000; Forbes & Lin 2000). In a more realistic corona, on the other hand, the local Alfvén speed decreases with height at large altitudes, the erosion of the sheet is not very fast and may go on for quite a long time (Lin 2002). The difference between the results of Lin & Forbes (2002) and those of Lin (2002) confirms that the behavior of growing flare loops are not determined by the strength of magnetic field as suggested by Švestka (1996), instead it is governed by the rate of magnetic reconnection near the current sheet which is controlled by the local Alfvén speed.

Another important morphological feature of CME related to the reconnecting current sheet is the rapidly expanding CME bubble during the eruption. Lin et al. (2004) and Lin & Soon (2004) found that the closed magnetic field does not need to open completely in a plausible eruptive process, in order that a large amount of the reconnected magnetic flux and plasma is brought during the eruption into the outermost corona and interplanetary space. They found that, like the flare/CME loop/giant arch system, the separatrix bubble that surrounds the flux rope (refer to the region inside the red shell in Fig. 4), together with the hot plasma inside, is a product of magnetic reconnection. As the magnetic reconnection sends more and more plasma and magnetic flux into the separatrix bubble, the bubble swells very rapidly (i.e., much faster than the adiabatic expansion of the flux rope). The "flux rope" that is often observed by coronagraphs may actually be the rapidly expanding separatrix bubble.

Their calculations showed that the magnetic flux ejected into the heliosphere by CMEs consists of two components, one due to the toroidal magnetic field and one due to the poloidal field. The flux contributed by the toroidal field mainly exists in the flux rope prior to the eruption. For typical eruptions, they found the value of the magnetic flux due to the toroidal field to be 6.53×10^{20} Mx, while the values estimated according to the observational data of Lepping et al. (1990, 1997) and Webb et al. (2000) range from 4.55×10^{20} to 1.46×10^{22} Mx. As for the magnetic flux due to the poloidal field, their work indicated that there are several sources, but the observations are not able to distinguish them. In situ measurements gave a total amount of the poloidal flux from all sources varying from 3.35×10^{21} to 2.68×10^{22} Mx, while the theory gave a few times 10^{22} Mx.

Furthermore, they pointed out that the outflow of reconnected plasma and magnetic flux leaves the reconnection site through both tips of the current sheet. The downward flow eventually reaches the chromosphere and causes the latter to evaporate, creating bright flare loops and ribbons. The upward flow is eventually sealed inside the separatrix bubble, creating a rapidly expanding structure that observers usually identify as the flux rope. The plasma in the upward flow fills the outer shell of the separatrix bubble and probably causes the separatrix bubble to show the three-component feature of CMEs.

The plasma injection into the CME bubble may also be indirectly confirmed by radio observations. Figure 5 shows a set of composites (from Wang et al. 2006) of the MDI magnetograms and the radio emission contours at 164 MHz obtained by the Nançay Radioheliograph (NRH) for the 2000 July 14 event. The evolution in the radio emission contours suggests an expanding structure. Comparisons with the images in other wavelengths indicate that the expanding structure shown in Figure 5 was the radio counterpart of the optical CME observed by various other instruments (Wang et al. 2006). Considering the fact that the radio

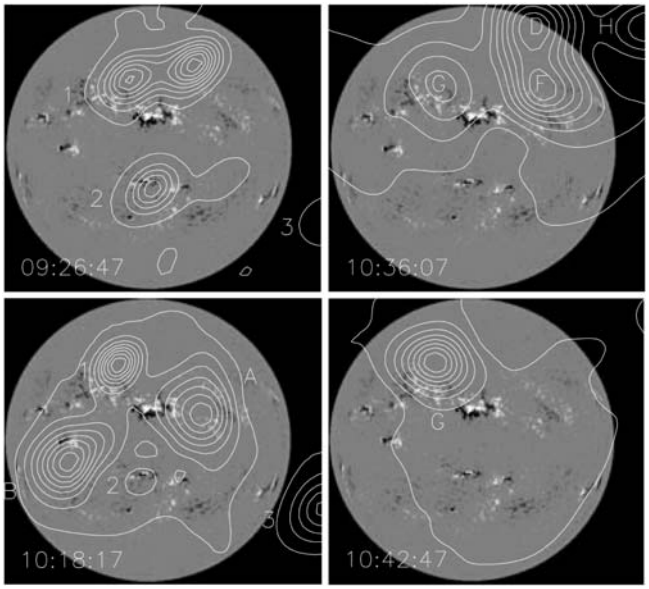

Fig. 5 Composite of the radio emission contours at 164 MHz obtained by the Nançay Radioheliograph (NRH) and the MDI magnetograms of the 2000 July 14 event. Field of view of the NRH contours is $5.5' \times 3.2'$, from Wang et al. (2006).

emission observed by NRH at fixed frequency depends solely on the plasma density, we realize that the change in the plasma density of the above expanding structure was not significant. This implies that either the expansion was non-adiabatic, rather, it was a kind of successive piling-up of magnetized materials with similar density, or a continuous injection of plasma into the expanding structure. In fact, the works by Lin et al. (2004) and Lin & Soon (2004) showed that both processes may occur simultaneously in the eruption. Observations by Maia et al. (2007) support this scenario.

However, more detailed computations are definitely required to confirm the proposed identifications. In particular, Lin et al. (2004) and Lin & Soon (2004) simply assumed that plasma is injected into the outer shell of the CME bubble at a high enough speed so that it is evenly distributed around the shell as indicated by the cartoon of Figure 4. A more modest injection speed would lead to a lower density at the CME front and a U- or V-shaped structure at the top of the current sheet. Now, U- or V-shaped structures are indeed observed in at least 10% of CMEs and are generally classified as coronal disconnection events (Webb et al. 2003). More detailed computations will also help to clarify the amount of heating involved and whether the injected plasma ought to appear in high-temperature lines, such as [Fe XVIII], as observed in some fast CMEs (Raymond et al. 2003).

5 OBSERVATIONAL FEATURES OF RECONNECTING CURRENT SHEETS IN ERUPTIONS

As indicated by the cartoon in Figure 4, the model of Lin & Forbes (2000) further predicts that with the magnetic energy around the current sheet being converted into thermal and kinetic energy, the plasma flows along the current sheet both upward and downward at approximately the local Alfvén speed and is heated to a high temperature. This implies that we should be able to observe hot plasma flows both leaving and approaching the Sun along the current sheet during an eruption that gives both a flare and a CME.

Because the current sheet is usually confined in a pretty narrow streamer-like region and magnetic reconnection always produces hot plasma inside the current sheet, it is almost impossible to be directly detected by traditional ground-based observations, and it is also very hard to be observed in space (see the introduction of Ko et al. 2003 for a brief overview). So, it was not until McKenzie & Hudson (1999) and McKenzie (2000), that some properties of magnetic reconnection in the current sheet were investigated.

5.1 Downward Reconnection Outflows

McKenzie & Hudson (1999) identified, for the first time, the apparent mass motion above the post-flare loop system. The flare was observed by *Yohkoh* on 1999 January 20. This long-duration event displayed a group of growing post-flare loops associated with a CME and large-scale mass motions toward the Sun along the current sheet over the flare loops. Comparing the images given by them with the cartoon in Figure 4, we believe that McKenzie & Hudson (1999) observed that current sheet exactly face-on, or nearly so. The current sheet showed a fan of spike-like ray structure that had been seen before (Švestka et al. 1998) by *Yohkoh*, but the January 20 event displayed a much clearer view of the mass motions. They found that the late-phase downward motion was in the form of soft X-ray dark voids at speeds varying from 100 to 200 km s^{-1}, that the temperature in this region reached up to 9.1×10^6 K, and that the density was a few times 10^9 cm^{-3}. These data indicate that the dark X-ray voids are blobs, or magnetic islands in the reconnecting sheet. Another 11 examples of similar Sun-ward flows were also reported by McKenzie (2000) in the long-duration events observed by *Yohkoh* SXT. The speeds of those flows ranged from 50 to 500 km s^{-1}, and all the events were associated with CMEs.

Following the above works, a succession of three similar events were observed. Sheeley & Wang (2002) reported coronal downflows observed with LASCO at $2-6\,R_\odot$ from the heliocenter. The maximum velocities of individual downflows varied from 50 to 100 km s^{-1}. The well-studied TRACE event occurring above the west limb on 2002 April 21 provided many authors a good opportunity of investigating in detail reconnection outflows towards the Sun. This event developed an X1.2 class flare and a very fast CME (≥ 2500 km s^{-1}), and was also well observed by the instruments on *SOHO*, including LASCO, SUMER, and UVCS (Innes et al. 2003; Raymond et al. 2003; Sheeley et al. 2004). The downward flow features were observed at the early stage of the eruption, so, both the speed and temperature of the plasma flow were fairly high, reaching 1000 km s^{-1} and a few 10^7 K, respectively.

Sheeley et al. (2004) employed a technique which he had developed to study motions in the outer corona (see Sheeley et al. 1999) to track the plasma downflows in the same event. What is nice about this technique is that it makes manifest a couple of important features related to magnetic reconnections atop flare loops. These features include the fast reconnection outflow ($100 - 600$ km s^{-1}) and the significant deceleration (~ 1500 m s^{-2}) as the flow approaches the top of the closed flare loop. Such a deceleration is highly suggestive of production of the termination shock on the top of flare loops (see Fig. 4 and Forbes & Acton 1996).

Asai et al. (2004) presented a detailed study of downward motions above flare loops observed in the 2002 July 23 event. This event produced an X4.8 flare and an energetic CME (~ 2600 km s^{-1}), and was well observed by TRACE, RHESSI, NoRH, UVCS and LASCO (Emslie et al. 2003; Raymond et al. 2003). In this case, the downflows above the post-flare loops were seen not only in the decay phase but also in the impulsive and main phases, and showed clear correlation with the non-thermal emissions in microwaves and HXRs. Magnetic reconnection was thought to account for these characteristics. Considering the fact that this X4.8 flare was also associated with an energetic CME, we believe that the downward flows and their related emission features observed in various wavelengths displayed typical manifestations of energy release occurring in a major eruptive process similar to those described by the model shown in Figure 4.

Downward motions near the top of the loop systems were also seen in RHESSI hard X-ray ($25 - 50$ and $12 - 25$ keV) and soft X-ray ($6 - 12$ keV) observations (Sui & Holman 2003; Sui et al. 2004). In the three events investigated by Sui & Holman (2003) and Sui et al. (2004), the hot loops or the loops observed in high energy ($12-25$ or $25-50$ keV) band were located above those in low energy band ($6-12$ keV), the loop tops in both bands showed apparent downward motions at the beginning of the hard X-ray impulsive phase. The speeds of the downward motion varied from 8 to 23 km s^{-1}, and the loops in the high energy band moved faster than those in the low energy band. Similar motions were also confirmed by observations of flare radio loops at frequencies of 17 and 32 GHz, and TRACE 195 Å loops (e.g., Li & Gan 2005, 2006). Such a motion pattern is different from the reconnection outflow toward the Sun. Sui et al. (2004) suggested that it is due to the evolution in the shape of the current sheet itself (the current sheet stretches downward somehow).

However, Lin (2004a) pointed out that this motion occurred outside the current sheet though it was very close to the lower tip of the sheet, and suggested an alternative process to account for the motion, namely,

the process known as shrinkage of post-flare loops (Švestka et al. 1987; Lin et al. 1995; Forbes & Acton 1996; Lin 2004a). In this process, the closed field lines where the flare loop is believed to lie never stayed at the positions where they were produced, but moved downward to a lower height closer to the potential state. At the early stage of the flare (i.e., beginning of the hard X-ray impulsive phase), shrinkage of individual newly formed flare loops is much more significant than the growth of the loop system (Lin 2004a). When the two motions combine together, the faster component dominates the result if they are not distinguishable. So the downward motions at the top of flare loop system observed by Sui et al. (2004) are quite likely due to the shrinkage of the newly formed loops at the early stage of the eruption.

5.2 Upward Reconnection Outflows

Reconnection outflow leaving the Sun along the current sheet was first analyzed by Ko et al. (2003) although this was not the first time it was observed (see Webb et al. 2003; Simnett 2004), and the development of the sheet in major eruptions had been confirmed by Akmal et al. (2001) and Ciaravella et al. (2002). The event reported by Ko et al. (2003) took place on 2002 January 8 and gave rise to a fast CME ($1800\,\mathrm{km\,s^{-1}}$) and a group of soft X-ray loops (the main part of the flare was behind the disk, so its class was difficult to determine). What is nice about this event is that the sheet above the flare loops was observed roughly edge-on, which allowed the detectors to receive enough emission data for a reliable diagnostics of the plasma properties inside the sheet. Combining the data from UVCS, EIT, LASCO, CDS, as well as from the MK4 coronameter at the Mauna Loa Solar Observatory (MLSO MK4), Ko et al. (2003) investigated the morphological and dynamical properties of this event. The plasma outflows leaving the Sun could be recognized by a group of moving plasma blobs along the sheet seen in the LASCO images (movies). These blobs moved at speeds ranging from 300 to $650\,\mathrm{km\,s^{-1}}$. The presence of highly ionized ions, such as FeXVIII and CaXIV, in the sheet suggests a temperature as high as $(3 \sim 6) \times 10^6$ K. The composite of the EIT 195 Å images and MK4 images replicated the standard Kopp-Pneuman configuration of the two-ribbon flares (Kopp & Pneuman 1975, and also see Fig. 3). By assuming that the magnetic energy near the current sheet was equally converted into the kinetic energy and thermal energy, they deduced that the magnetic field near the sheet varied from 0.47 to 1.2 G.

Encouraged by the success of Ko et al. (2003) in the study of the current sheet and the associated magnetic reconnection process, Lin et al. (2005) investigated the event occurring on 2003 November 18. This event took place on the east limb of the Sun and developed an energetic partial halo CME ($\sim 2000\,\mathrm{km\,s^{-1}}$), a long current sheet and a group of bright flare loops in the wake of the CME. It was observed by several instruments both in space and on the ground, including EIT, UVCS, LASCO, RHESSI, as well as MK4. The sheet was also observed edge-on. Combining the data from these instruments, Lin et al. (2005) analyzed various properties of the eruptive process, including those around the sheet. The most important aspect of the work of Lin et al. (2005) is that the UVCS data were used to deduce the speed of the reconnection inflow near the sheet. The intention to measure the speed around the reconnection site was first indicated by Yokoyama et al. (2001), who studied both the SOHO/EIT and the *Yohkoh*/SXT images around the cusp structure on the top of flare loop system, and noticed a nice cusp-shaped loop and a plasma blob in the SXT images (movies), and also a bubble-like void ejection in the EIT 195 Å images (movies). The core of this void is dark in EUV and bright in soft X-ray, which implied a temperature of about 4×10^6 K. As the void moved away from the limb, an X-shaped structure formed behind it and a clear merging pattern of threads towards the X-point could be seen. They believed that this merging pattern tracked the reconnection inflow near the reconnection site. The measured speeds of the merging motions shown in the EIT 195 Å movies brought the reconnection inflow velocity to the range from 1.0 to $4.7\,\mathrm{km\,s^{-1}}$.

However, the structure seen in the EIT 195 Å images (movies) is diffuse, from which it is difficult to determine an accurate speed. Moreover, Chen et al. (2004) re-analyzed the observations of Yokoyama et al. (2001), and found that the apparent motions towards the X-point was actually due to a changing of the position of the reconnection site rather than inflow. So, Lin et al. (2005) chose to use the UVCS observations to determine the inflow speed, and found that the speed of reconnection inflow near the current sheet varied from 10.5 to $106\,\mathrm{km\,s^{-1}}$. These values are apparently larger than those deduced by Yokoyama et al. (2001).

Another disadvantage of the work of Yokoyama et al. (2001) is that the local Alfvén speed near the sheet, which governs the rate of magnetic reconnection, was not measured directly. Instead, it was estimated from the soft X-ray emission measure by assuming that all the magnetic energy released during the eruption

went to heating via reconnection, and that the depth (L) of the source region along the line-of-sight was on the same order of length of the flare loops so that the source region of the soft X-ray emission fills the whole volume of L^3 when calculating the electron density. These two assumptions led to uncertainties in their results: The first assumption obviously causes the magnetic field near the reconnection site to be underestimated because much (perhaps as much as half) of the released energy goes to kinetic energy of the reconnected plasma flows, and the second assumption leads to the total thermal energy being overestimated because the source region of soft X-ray could never fill the whole volume of L^3.

To avoid such uncertainties, Ko et al. (2003) and Lin et al. (2005) chose to estimate the local Alfvén speed around the reconnection region by measuring the speed of the reconnection outflow directly. The standard theory of magnetic reconnection indicates that these two speeds are equal (Priest & Forbes 2000). Because the current sheet developed by the event of 2003 November 18 was also observed edge-on, the features of the reconnection outflow could be easily seen. Lin et al. (2005) recognized several blobs in the outflow and five of them were clearly recognized. Investigating the temporal behaviors of these blobs brought the speed of reconnection outflow leaving the Sun to the range from 460 to 1075 km s^{-1}. Comparing these values with those of the inflow speed brings the rate of magnetic reconnection to the range from 0.01 to 0.23.

Recently, Narukage & Shibata (2006) reported observations of reconnection inflows near the reconnection site after analyzing the EIT data for a set of events. They surveyed the events observed by EIT from 1996 to 2000 and recognized six events that manifested apparent reconnection inflows. The approach used by Yokoyama et al. (2001) to deduce the speed of the reconnection inflow was improved, and the inflow speed measured using the new method was larger than the previous ones by a factor of 2.5. Correspondingly, Narukage & Shibata (2006) found that the rate of magnetic reconnection for the events studied, including the one investigated by Yokoyama et al. (2001), varied from 0.001 to 0.07. This result is consistent with those obtained by other authors (e.g., see table 4 of Narukage & Shibata 2006).

5.3 Internal Structure and Thickness of the Reconnecting Current Sheet

The high electrical conductivity and force-free environment in the corona confines the reconnection region to a thin layer, so a long and thin current sheet is expected to develop in major eruptive processes. This feature of reconnecting current sheet allows us to treat the current sheet as an infinitely thin line when the main purpose is to study the global behavior of the eruption (e.g., Lin & Forbes 2000). Although indirect evidence indicates the existence of current sheet in eruptions (e.g., see Forbes & Acton 1996 for a brief review), direct observation of a thin current sheet is difficult. This is because both the size and emission of the current sheet are easily dominated by other large-scale structures nearby (e.g., see Ko et al. 2003 for detailed discussion).

So, it is often assumed that the current sheet is too thin to be observable since its thickness, d, is believed to be limited by the proton Larmor radius (Litvinenko 1996; Wood & Neukirch 2005; and references therein), which amounts to a few tens of meters in the coronal environment. This view is based on information on small-scale (meter size) magnetic reconnection in the laboratory. When the sheet forms in the solar eruption, on the other hand, it could develop in length at a speed of a few hundred km s^{-1} (Forbes & Lin 2000; Lin & Forbes 2000; Lin 2002). In such a highly dynamic process, the Larmor radius of the particles cannot govern the scale of the magnetic structure. Instead, various plasma instabilities will likely occur and play an important role in diffusing the magnetic field and in governing the scale of the sheet (Strauss 1986, 1988).

Both theories (e.g., Furth et al. 1963; Strauss 1986, 1988; Bhattacharjee & Yuan 1995; Priest & Forbes 2000) and numerical experiments (Ambrosiano et al. 1988; Drake et al. 2006; Riley et al. 2007) indicate that a long current sheet can easily become unstable to tearing mode turbulence. When turbulence occurs, the current sheet is torn to many small scale magnetic islands or turbulence eddies (see figs. 6.1 and 6.3 of Priest & Forbes 2000). Formation of the magnetic islands widens the current sheet apparently (Strauss 1986 and 1988). Furthermore, annihilation caused by the tearing mode turbulence dissipates magnetic energy in a very efficient way (Bhattacharjee & Yuan 1995). This implies that reconnection may be able to take place at a reasonably fast rate even if the sheet is thick.

Recently, Lin et al. (2007) analyzed a set of unique data for three eruptions observed by the UVCS and LASCO experiments on *SOHO*. They found that, in some circumstances, the current sheets are observable,

and their thickness in real events may range from 10^4 to 10^5 km. The results imply that large-scale plasma turbulence is operating within the sheets during the eruption, and pose a serious challenge to the existing theories of reconnection and particle accelerations in the sheet.

The internal structures of the sheet may also be manifested indirectly by the location of the coronal X-ray emission sources above flare loops (Sui et al. 2006), and by the time profiles of both the subsecond pulses of the hard X-ray emission (e.g., see Aschwanden 2004a and references therein) and the quasi-periodic reversals of the radio polarizations at frequency of 17 GHz (e.g., Huang & Lin 2006 and references therein). These results reveal the role of magnetic reconnection in solar flares from the way the particles are accelerated in the sheet: they implicitly suggest the existence of fine structures inside the reconnecting current sheets. Such structures could be caused either by plasma instability (turbulence) or by the fact that the reconnection process in the sheet is not uniform in either space or time. In the recent work by Lin et al. (2007), properties of the tearing mode instability were used to estimate the thickness of the current sheets from the observations.

6 CORRELATIONS OF CMES WITH SOLAR FLARES AND ERUPTIVE PROMINENCES

Correlation between solar flares and CMEs was first discussed by Gosling et al. (1976) based on Skylab observations, and then by MacQueen & Fisher (1983) and Harrison (1986) based on the K-coronameter data, more recently by Dere et al. (1999), Neupert et al.(2001), and Zhang et al. (2001b) based on LASCO observations, and by Alexander et al. (2002) based on both LASCO and Yohkoh observations. Zhang et al. (2001b) showed that the early impulsive acceleration phase of CMEs coincides with the rise of the associated X-ray flares, and the increase in the CME speed always corresponds to an increase of the soft X-ray flux. Related to this correlation is the classification of CMEs, and the mechanisms for various observed CMEs. Speed is the usual criterion to distinguish two types of CMEs: slow (gradual) CMEs and fast (impulsive) CMEs. Slow CMEs normally show gentle and continuous propagations with speeds less than 500 km s^{-1} and maximum acceleration less than 100 m s^{-2} (Srivastava et al. 1999); while fast CMEs usually manifest energetic behaviors with speeds greater than 500 km s^{-1} and maximum acceleration over 100 m s^{-2}, while speeds exceeding 2000 km s^{-1} and maximum of accelerations larger than 1000 m s^{-2} have also been reported (Zhang et al. 2001b; Alexander et al. 2002; Raymond et al. 2003).

While many authors tried to find and discuss differences between CMEs that are, and those that are not, associated with flares (e.g., Gosling et al. 1976; MacQueen & Fisher 1983; Kahler 1992; Dryer 1996; Sheeley et al. 1999; Andrews & Howard 2001), Švestka (1986) was the first to point out that in both cases the cause of the CME is the same, the only difference between them is the strength of the magnetic field in the region where the eruption is initiated (see also Švestka & Cliver 1992; Švestka 1995), and that the correlations between solar flare and CME vary continuously with the strength of the relevant magnetic field (Z. Švestka 2002, private communication) and there is no sharp boundary separating good and poor correlations. The event observed by Goff et al. (2005) provides a clear support to this statement. This event was observed by a variety of instruments, including the CDS and LASCO on board *SOHO*, TRACE and RHESSI. It included a slow CME with a speed of around 130 km s^{-1}, and a growing flare loop system with a rising hard X-ray source on the top. The work of Vršnak et al. (2005) provides further support to Švestka's statement.

After having analyzed 545 flare-related CMEs and 104 non-flare CMEs, Vršnak et al. (2005) found that both data sets show quite similar characteristics, in disagreement with the concept of two distinct (flare/non-flare) types of CMEs. They noticed that, while it is true that CMEs associated with major flares are on average faster and broader than non-flare and/or small-flare CMEs, and that a well-defined correlation between the CME speed and the flare importance could be established, many characteristics manifested by the non-flare CMEs were found quite similar to those shown by the CMEs associated with B- or C-class X-ray flares, which is suggestive of a "continuum" of events, rather than distinct species. A similar conclusion was drawn recently by Bao et al. (2006).

Zhang et al. (2002) were the first to have quantitatively investigated the correlation between CMEs and solar flares via variation of the time of flare maximum with the speed of the associated CME. By analyzing the flare data from TRACE, the CME data from LASCO, as well as the GOES X-ray flux data used to determine the times of flare maxima, they found that the faster the CME is, the earlier the associated flare reaches its maximum, and that the association with flares is better and more apparent for fast than slow

CMEs. Among the samples they chose, most X-class flares (12 out of 13) went with fast CMEs, more than half (18 out of 30) fast CMEs in turn are associated with M-class flares, and only one X-class flare was associated with slow CME.

In a similar study, Moon et al. (2002) found that the fraction of CMEs associated with flares among a total of 3217 CMEs tends to increase with the CME speed: less than 5% of slow ($\leq 200\,\mathrm{km\ s^{-1}}$) CMEs were associated with flares, and the fraction approaches 15% as the CME speed reaches $1000\,\mathrm{km\ s^{-1}}$. However, these fraction values can only be considered as lower limits since Moon et al. (2002) used a very strict way of selecting their samples that ruled out CMEs associated with both flares and eruptive prominences. However, their conclusion just replicates that of Zhang et al. (2002) in another way. The above correlation equally holds for eruptions that occurred during the solar minimum: slow CMEs are poorly associated with other activities on the surface, the average speed of the CMEs with firmly associated activity is clearly higher than that of the unassociated CMEs (Wagner 1984; St. Cyr & Webb 1991).

On the basis of the catastrophe model of CMEs developed by Forbes & Priest (1995), Lin & Forbes (2000), and Lin (2002), Lin (2004b) incorporated the effect of gravity in the calculations and studied the relationship between CMEs and the associated flares, and found that the flares associated with fast CMEs reach maxima earlier than those associated with slow CMEs. This result is consistent with that of Zhang et al. (2002), deduced from observations. Lin (2004b) also noticed that the correlation of CME with the associated flare is governed by the free energy in the magnetic structure that is available for driving the eruption: greater free energy goes with closer correlation, and conversely. Because the free energy is related to the second power of the background field, the results of Lin (2004b) thus theoretically confirmed Švestka's conclusion.

After re-analyzing the results of a number of previous works on CMEs and eruptive prominences, Lin (2004b) realized that the correlation between CMEs and eruptive prominences does not include so many physical issues as that between CMEs and flares. The former is simply dependent on the mass distribution and/or concentration in the disrupting magnetic field: if the disrupting field contains enough mass ($> 5\times10^{15}$ g, the average mass of CMEs) that is significantly concentrated, then the CME commences with eruptive prominence, otherwise, the CME develops without an apparent associated eruptive prominence.

7 START FREQUENCY AND ONSET POSITION OF TYPE II RADIO BURSTS

In a major solar eruption, a huge amount of magnetized plasma and energy may be flowing into the outermost corona and interplanetary space at considerable speeds, say a few $10^3\,\mathrm{km\ s^{-1}}$ (e.g., Forbes 2000; Klimchuk 2001; Priest & Forbes 2002; Lin et al. 2003). As the bulk of magnetized plasma (CME) propagates through the corona at high speed, it is very likely to induce and drive a fast-mode shock ahead of it like a piston when its velocity exceeds the local magneto-acoustic speed (or the Alfvén speed in the force-free environment that is the solar corona). The long duration gradual solar energetic particle events (see Lee 2005 for a review), the type II radio bursts observed during major eruptions (Cane et al. 2002; Vourlidas 2004; Gopalswamy 2004a,b), as well as the broadening and the Doppler dimming shown by the spectral profiles of OVI and Lyα lines (Raymond et al. 2000; Mancuso et al. 2002) all provide convincing evidence for the passage and propagation of CME-driven shocks. A recent statistical study by Mancuso & Raymond (2004) further suggests that all type-II radio bursts might be piston-driven, originating at the top or flanks of CMEs.

Observations of type II and III bursts indicate that while type III bursts may appear at any altitude from the very low corona (corresponding to GHz frequency) to interplanetary space (kHz frequency), type II bursts do not behave the same way: the reported highest frequencies of the fundamental components of type II bursts usually do not exceed a few hundred MHz (e.g., see Kundu 1965; Zlotnik et al. 1998; Klassen et al. 2000; Dulk et al. 2000; Cane et al. 2002; Klassen et al. 2003; Mann et al. 2003). This suggests a minimum altitude for the excitation of type II emission. On the basis of the empirical model of plasma density in the corona of Sittler & Guhathakurta (1999), the frequency of 200 MHz corresponds to an altitude of 0.37 $R_\odot$ or 2.6×10^5 km from the solar surface.

On the basis of previous works, Lin et al. (2006) found that whether CME-driven shocks occur, and if so, when and where, and hence the type II radio bursts, depend on both the magnetic field strength σ and the rate of reconnection M_A for the given plasma density distribution in the corona. With a strong magnetic field and a fast reconnection, type II radio bursts are induced at a low altitude with a high start

frequency. For a major eruption that develops a CME with a terminal speed of around 1000 km s $^{-1}$, they found the onset position of the type II radio burst to be at around 0.5 $R_\odot$, corresponding to a start frequency of the fundamental lane of 150 MHz. B. Vršnak (2006, private communication) suggested that the value of 150 MHz might be too high for an altitude of $0.5R_\odot$, and that 110 MHz seems more appropriate. Of cause, this is also dependent on the model of the coronal plasma density we chose.

The roles of M_A and σ roughly compensate each other in their effect on the above properties of type II radio bursts, but the onset position is more dependent on M_A than on σ. Complex functional behavior of the CME velocity relative to the Alfvén speed determines that even fast CMEs (> 800 km s $^{-1}$) may not be able to produce type II radio bursts if M_A is not large enough. Examples of radio-quiet fast CMEs have been reported by many authors (e.g., see Gopalswamy 2004b).

Although both theory and observations indicate that the CME is very likely the driver of the shocks that ignite the type II burst in the eruptive process, it is hard to rigorously prove that all coronal shocks observed are driven by CMEs (Cane & Ericson 2005; Pohjolainen & Lehtinen 2006; Vršnak et al. 2006). The detailed process through which the shock that produces the type II radio burst may be ignited is still a subject of active research. Most recently, T. Bastian (2006, private communication) mentioned that a short period type II burst without associated CME was observed with the start frequency of the fundamental lane between 700 and 800 MHz. Such example is very rare, but it indicates that no hard and fast conclusions about the origin of type II burst-driven shocks should yet be drawn.

8 SUMMARY

The large-scale magnetic structures related to eruptive phenomena in the solar atmosphere usually exist in the form of filaments or filament channels in the corona prior to the eruption. A helical organization in these structures allows the filament material to accumulate and float in the corona, and implies the existence of electric current flowing along tangling strands inside the filament, which provides a buoyancy or magnetic compression that pushes the filament upward. The magnetic field lines that pass over the top of the filament and with their footpoints anchored in the photosphere produce a magnetic tension that pulls the filament downward. Equilibrium in the system is realized when the forces of magnetic compression and tension acting on the flux rope balance each other. In the framework of the catastrophe theory, the filament is usually modeled by a current-carrying flux rope in which electric current and filament material are co-located. This is done for mathematical convenience although observations in some circumstances do show the co-location.

Ceaseless mass motion in the photosphere drives the coronal magnetic field through a succession of quasi-static equilibrium states held by a balance between magnetic tension and compression, converting the kinetic energy of mass motion into the magnetic energy stored in the coronal magnetic field. Motions in the photosphere that displace the footpoints of the coronal magnetic field could be of the form of shearing, converging, twisting, or any combination of these. Both theory and observations further indicate that the shearing and converging motions of the footpoints are also responsible for the formation of the filaments or the prominences as a type of energy conversion and transportation. We realize also that new emerging magnetic flux and interactions among different magnetic systems (or active regions) are another two important processes that can enhance greatly the complexity of the coronal magnetic field and increase its free energy.

Evolution of the system becomes dynamic when catastrophic loss of equilibrium takes place and the filament is thrust upward as tension loses out to compression. Development of the current sheet during the catastrophe makes it possible for the magnetic field in the coronal environment of high electrical conductivity to dissipate at a reasonably fast rate, and the fast dissipation of the field directly results in the growing flare loop system in the low corona and in the rapidly expanding CME bubble propagating through the outermost corona and interplanetary space. In the coronal environment where magnetic field is strong and magnetic forces are all important, the impact of plasma gas pressure on the eruption is comparatively tiny, and that of the gravity of the filament, negligible.

The high electrical conductivity and the force-free environment in the corona confine the current sheet in the eruption to a small localized region, compared to other nearby bright features. This makes direct observation of the reconnecting sheets very hard. It is only recently that observations and the subsequent analyses have confirmed the formation and development of the sheets in eruptions. Further results indicate that the sheet could actually be quite thick as a result of plasma instabilities and turbulence, and could be

seen directly when viewed edge-on. For the time being, however, it is impossible to guarantee that the sheet in every single event is observed edge-on. This is why, on one hand, we have observed so many CME/flare events and recognized various pieces of indirect evidence for reconnection geometry and processes (see e.g., Aschwanden 2004b), and, on the other, only a very few of them were observed well enough to provide direct evidence of magnetic reconnection. We expect this problem will be resolved when observations from STEREO become available.

Fast CMEs are always associated with major flares because they both need the support of rapid energy conversion through fast magnetic reconnection in the current sheet. The current sheet connects them, forming a system that involves the disruption and re-organization of the coronal magnetic field, and the transportation of magnetic flux and plasma. Behind the CME-flare association is the magnetic free energy that is available for driving the eruption, and this energy is directly governed by the strength of the relevant background field. Investigations show that the stronger the background field is, the more apparent the association is.

When the speed of the CME front exceeds the local magneto-acoustic speed (or the Alfvén speed in the force-free environment), a CME-driven shock, and hence a type II radio burst, is expected. The start frequency of the type II radio bursts helps determine the onset altitude of the CME-driven shock if the distribution of the plasma density in the corona is known, and the onset position of type II bursts can, in turn, be calculated for a given CME and a given plasma density model. The fact that the CME start from a motionless state determines a lowest altitude where the type II radio burst commences. Theoretical calculations show that the onset of type II bursts in a typical eruption should occur at around 0.5 $R_\odot$ from the solar surface with a start frequency of the fundamental component of about 150 MHz. This result is consistent with similar estimates of a few hundred MHz based on the observations.

It is also worth pointing out that the cause of the type II burst, however, especially the metric type II burst, is still an open question. Recent works by Cane & Erickson (2005), Pohjolainen & Lehtinen (2006) and Vršnak et al. (2006) investigated various eruptive events, and noted that the CME might not be the driver of the shocks that ignite the type II bursts although there are also problems if those shocks are not driven by CMEs. Thus, further investigations on this issue are definitely needed.

Acknowledgements This work was supported by the Ministry of Science and Technology of China under the 973 Program grant 2006CB806303, and by the National Natural Science Foundation of China under grant 40636031 to the Yunnan Astronomical Observatory. The author's work at CfA was supported by NASA under grants NNX07AL72G to the Smithsonian Astrophysical Observatory.

References

Akmal A., Raymond J. C., Vourlidas A., Thompson B., Ciaravella A., Ko Y.-K., Uzzo M., Wu R., 2001, ApJ, 553, 922
Alexander D., Metcalf T. R., Nitta N. V., 2002, Geophys. Res. Lett., 29 (10), 10.1029/2001GL013670
Aly J. J., 1991, ApJ, 375, L61
Amari T., Luciani J. F., Aly J. J., Mikić Z., Linker J., 2003, ApJ, 585, 1073
Ambrosiano J., Matthaeus W. H., Goldstein M. L., Plante D., 1988, J. Geophys. Res., 93, 14383
Andrews M. D., Howard R. A., 2001, Space Sci. Rev., 95, 147
Antiochos S. K., DeVore C. R., Klimchuk J. A., 1999, ApJ, 510, 485
Asai A., Yokoyama T., Shimojo M., Shibata K., 2004, ApJ, 605, L77
Aschwanden M. J., 2004a, ApJ, 608, 554
Aschwanden M. J., 2004b, Physics of the Solar Coronal − An Introduction, Chichester: Praxis Publishing
Aulanier G., Srivastava N., Martin S. F., 2000, ApJ, 543, 447
Bao X., Zhang H., Lin J., Stenborg G. A., 2007, A&A, 463, 321
Bhattacharjee A., Yuan Y., 1995, ApJ, 449, 739
Cane H. V., Erickson W. C., 2005, ApJ, 623, 1180
Cane H. V., Erickson W. C., Prestage N. P., 2002, J. Geophys. Res., 107(A10), 1315
Canfield R. C., Blais K. A., Reardon K. P., Acton L. W., Kurokawa H., 1994, in Solar Active Region Evolution: Comparing Models with Observations, edited by K. S. Balasubramaniam, G. W. Simon, ASP, San Francisco, p. 411
Carmichael H., 1964, in The Physics of Solar Flares, ed. W. N. Hess, Washington: NASA, 451

Chase R. C. et al., 1976, in COSPAR Space Research XVI, Proceedings of the Open Meetings of Working Groups on Physical Sciences, May 29-June 7, 1975, and Symposium and Workshop on Results from Coordinated Upper Atmosphere Measurement Programs, Varna, Bulgaria, May 29-31, 1975. (A77-23951 09-88) (Berlin, East Germany, Akademie-Verlag GmbH), p.917
Chen P., Shibata K., 2000, ApJ, 545, 524
Chen P., Shibata K., Brooks D. H., Isobe H., 2004, ApJ, 602, L61
Chen Y., Li G., Hu Y., 2006, ApJ, 649, 1093
Ciaravella A., Raymond J. C., Li J., Reiaer P., Gardner L. D., Ko Y.-K., Fineschi S., 2002, ApJ, 575, 1116
Contarino L., Romano P., Zuccarello F., 2006, Astronomische Nachrichten, 327, 674
Dere K. P., Brueckner G. E., Howard R. A., Michels D. J., Delaboudiniere J. P., 1999, ApJ, 516, 465
Drake J. F., Swisdak M., Schoeffler K. M., Rogers B. N., Kobayashi S., 2006, Geophys. Res. Lett., 33, L13105
Dryer M., 1996, Solar Phys., 169, 421
Dulk G. A., LeBlanc Y., Bastian T. S., Bougeret J., 2000, J. Geophys. Res., 105, 27343
Emslie A. G., Kontar E. P., Krucker S., Lin R. P., 2003, ApJ, 595, L107
Feynman J., Martin S. F., 1995, J. Geophys. Res., 100, 3355
Forbes T. G., 2000, J. Geophys. Res., 105, 23153
Forbes T. G., Acton L. W., 1996, ApJ, 459, 330
Forbes T. G., Isenberg P. A., 1991, ApJ, 373, 294
Forbes T. G., Lin J., 2000, J. Atmos. Solar Terr. Phys., 62, 1499
Forbes T. G., Priest E. R., 1995, ApJ, 446, 377
Foukal P., 1971, Solar Phys., 19, 59
Gaizauskas V., Zirker J. B., Sweetland C., Kovacs A., 1997, ApJ, 479, 448
Goff C. P., van Driel-Gesztelyi L., Harra L. K., Matthews S. A., Mandrini C. H., 2005, A&A, 434, 761
Gopalswamy N., 2004a, in Solar and Space Weather Radiophysics: Current Status and Future Developments, eds., D. E. Gary, C. U. Keller, Boston: Kluwer, p.314
Gopalswamy N., 2004b, in The Sun and The Heliosphere as an Integrated System, eds., G. Poletto, S. T. Suess, Boston: Kluwer, p.222
Gosling J. T., Hildner E., MacQueen R. M., Munro R. H., Poland A. I., Ross C. L., 1976, Solar Phys., 48, 389
Harrison R. A., 1986, A&A, 162, 283
Heyvaerts J., Priest E. R., Rust D. M., 1977, Solar Phys., 216, 123
Hood A., W., Anzer U., 1990, Sol. Phys., 126, 117
Hu Y. 2004, ApJ, 607, 1032
Huang G., Lin J., 2006, ApJ, 639, L99
Innes D. E., McKenzie D. E., Wang T., 2003, Solar Phys., 217, 247
Isenberg P. A., Forbes T. G., Démoulin P., 1993, ApJ, 417, 368
Kahler S. W., 1992, Annu., Rev. Astron. Astrophys., 30, 113
Kiepenheuer K. O., 1953, in The Sun, ed. G. P. Kuiper, Chicago: Univ. of Chicago Press, p.322
Klassen A., Aurass H., Mann G., Thompson B. J., 2000, A&AS, 141, 357
Klassen A., Pohjolainen S., 2002, in Solar Variability: from Core to Outer Frontiers, A. Wilson, ed., ESTEC, Noordwijk, The Netherlands, ESA-SP 506, p.307
Klassen A., Pohjolainen S., Klein K.-L., 2003, Solar Phys., 218, 197
Klimchuk J. A., 2001, in Space Weather, ed., P. Song, G. Siscoe, H. Singer (Geophys. Monogr. 125; Washington: AGU), p.143
Ko Y., Raymond J. C., Lin J., Lawrence G., Li J., Fludra A., 2003, ApJ, 594, 1068
Kopp R. A., Pneuman G. W., 1976, Solar Phys., 50, 85
Kundu M. R., 1965, Solar Radio Astronomy, New York: John Wiley & Sons, USA
Kuperus M., 1996, Solar Phys., 169, 349
Kuperus M., Raadu M. A., 1974, A&A, 31, 189
Kurokawa H., Santo S., 2000, Adv. Space Res., 26, 441
Lee M. A., 2005, ApJS, 158, 38
Leighton R. B., 1964, ApJ, 140, 1547
Lepping R. P., Jones J. A., Burlaga L. F., 1990, J. Geophys. Res., 95, 11957
Lepping R. P., Szabo A., DeForest C. E., Thompson B. J., 1997, in Proc. 31st ESLAB Symp., Correlated Phenomena at the Sun, in the Heliosphere and in Geospace, ed. A. Wilson (Noordwijk: ESTEC, The Netherlands), p.163

Li Y., Gan W., 2005, ApJ, 629, L137
Li Y., Gan W., 2006, ApJ, 644, L97
Lin J., 2002, Chin. J. Astron. Astrophys. (ChJAA), 2, 539
Lin J., 2004a, Solar Phys., 222, 115
Lin J., 2004b, Solar Phys., 219, 169
Lin J., Forbes T. G., 2000, J. Geophys. Res., 105, 2375
Lin J., Forbes T. G., Priest E. R., Bungey T. N., 1995, Solar Phys., 159, 275
Lin J., Raymond J. C., van Ballegooijen A. A., 2004, ApJ, 602, 422
Lin J., Soon W., 2004, New Astron., 47, 53
Lin J., Soon W., Baliunas S. L., 2003, NewA Rev., 47, 53
Lin J., Ko Y.-K., Sui L., Raymond J. C., Stenborg G. A., Jiang Y., Zhao S., Mancuso S., 2005, ApJ, 622, 1251
Lin J., Li J., Forbes T. G., Ko Y.-K., Raymond J. C., Vourlidas A., 2007, ApJ, 658, L123
Lin J., Mancuso S., Vourlidas A., 2006, ApJ, 649, 1110
Lin J., van Ballegooijen A. A., 2005, ApJ, 629, 582
Linker J. A., Mikić Z., Lionello R., Riley P., Amari T., Odrstrcil D., 2003, J. Plasma Phys., 10(5), 1971
Liu Y., Jiang Y., Ji H., Zhang H., Wang H., 2003, ApJ, 593, L137
Litvinenko Y., 1996, ApJ, 462, 997
Livi S. H. B., Wang J., Martin S. F., 1985, Australian J. Phys., 38, 855
Low B. C., 1996 Solar Phys., 167, 217
Low B. C., 2001, J. Geophys. Res., 106, 25141
Lynch B. J., Antiochos S. K., MacNeice P. J., Zurbuchen T. H., Fisk L. A., 2004, ApJ, 617, 589
MacKay D. H., van Ballegooijen A. A., 2005, ApJ, 621, L77
MacKay D. H., van Ballegooijen A. A., 2006a, ApJ, 641, 577
MacKay D. H., van Ballegooijen A. A., 2006b, ApJ, 642, 1193
MacNeice P. J., Antiochos S. K., Philips A., Spicer D. S., DeVore C. R., Olson K., 2004, ApJ, 614, 1028
MacQueen R. M., Fisher R. R., 1983, Solar Phys., 89, 89
Mancuso S., Raymond J. C., 2004, A&A, 413, 363
Mancuso S., Raymond J. C., Kohl J. L., Ko Y.-K., Uzzo M., Wu R., 2002, A&A, 383, 267
Mann G., Klassen A., Aurass H., Classen H.-T., 2003, A&A, 400, 329
Maia D. J. F., Gama R., Mercier C., Pick M., Kerdraon A., Karlický M., 2007, ApJ, 660, 874
Martin S. F., 1990, in Dynamics of Quiescent Prominences, Lecture Notes in Physics 363, eds. V. Ruzdjak, E. Tandberg-Hanssen, Berlin: Springer, p.1
Martin S. F., Bentley R. D., Schadee A., Antalova A., Kucera A., Dezsö L., Gesztelyi L., Harvey K. L., Jones H., Livi S. H. B., 1984, Adv. Space Res., 4, 61
Martin S. F., Bilimoria R., Tracadas P. W., 1994, in Solar Surface Magnetism, eds. R. J. Rutten, C. J. Schrijver, New York: Springer-Verlag, p.303
Martin S. F., Dezsö L., Antalova A., Kucera A., Harvey K. L., 1982, Adv. Space Res., 2, 39
McKenzie D. E., 2000, Solar Phys., 195, 381
McKenzie D. E., Hudson H. S., 1999, ApJ, 519, L93
Mikić Z., Barnes D. C., Schnack D. D., 1988, ApJ, 328, 830
Mikić Z., Linker J. A., 1994, ApJ, 430, 898
Moon Y.-J., Choe G. S., Wang H., Park Y. D., Gopalswamy N., Yang G., Yashiro S., 2002, ApJ, 581, 694
Moore R. L., et al. 1980, in Solar Flares, ed. P. A. Sturrock, Boulder: Colorado Assoc. Univ. Press, p.341
Narukage N., Shibata K., 2006, ApJ, 637, 1122
Neupert W. M., Thompson B. J., Gurman J. B., Plunkett S. P., 2001, J. Geophys. Res., 106(A11), 25215
Poletto G., Kopp R. A., 1986, in The Lower Atmosphere of Solar Flares, ed. D. F. Neidig, NSO, Sunspot, NM, p.453
Pohjolainen S., Lehtinen N. J., 2006, A&A, 449, 359
Priest E. R., 1982, Solar Magnetohydrodynamics, Boston: Reidel, 56
Priest E. R., Forbes T. G., 2000, Magnetic Reconnection − MHD Theory and Applications, Cambridge: Cambridge Univ. Press
Priest E. R., Forbes T. G., 2002, A&A Rev., 10, 313
Priest E. R., Hood A. W., Anzer U., 1989, ApJ, 344, 1010

Priest E. R., Raadu M. A., 1975, Solar Phys. 43, 177
Qiu J., Wang H., Cheng C. Z., Gary D. E., 2004, ApJ, 604, 900
Raymond J. C., Ciaravella A., Dobrzycka D., Strachan L., Ko Y.-K., Uzzo M., Raouafi N.-E., 2003, ApJ, 597, 1106
Raymond J. C., Thompson B. J., St. Cyr O. C. et al., 2000, Geophys. Res. Lett., 27, 1439
Riley P., Lionello R., Mikić Z., Linker J. A., Clark E., Lin J., Ko Y.-k., 2007, ApJ, 655, 591
Rust D. M., 1972, Solar Phys., 25, 141
Rust D. M., 1973, Solar Phys., 33, 205
Rust D. M., 1975, in Optical and magnetic measurements of the photosphere and low chromosphere, paper presented at the Meeting on the Physics of the Solar Atmosphere, R. Soc. London
Rust D. M., Bridge III C. A., 1975, Solar Phys., 43, 129
Rust D. M., Roy J. A., 1974, in Environmental Research Papers, No. 474, Air Force Cambridge Res. Lab., Hanscom AFB, Mass
Rust D. M., Nakagawa Y., Neupert W. M., 1975, Solar Phys., 41, 397
Rust D. M. et al., 1980, in Solar Flares: A Monograph from Skylab Solar Workshop II, ed., P. A. Sturrock, Colo. Assoc. Univ. Press, Boulder, p.273
Schmieder B., Forbes T. G., Malherbe J. M., Machado M. E., 1987, ApJ, 317, 956
Schrijver C. J., DeRosa M. L., 2003, Solar Phys., 212, 165
Sheeley N. R. Jr., Bohlin J. D., Brueckner G. E., Purcell J. D., Scherrer V., Tousey R., 1975, Solar Phys., 40, 103
Sheeley N. R. Jr., Walters J. H., Wang Y.-M., Howard R. A., 1999, J. Geophys. Res., 104, 24739
Sheeley N. R. Jr., Warren H. P., Wang Y-M., 2004, ApJ, 616, 1224
Sheeley N. R. Jr., Wang Y.-M., 2002, ApJ, 579, 874
Simnett G. M., 2004, A&A, 416, 759
Sittler E. C. Jr., Guhathakurta M., 1999, ApJ, 523, 812
Srivastava N., Schwenn R., Inhester B., Stenborg G. A., Podlipnik B., 1999, in Solar Wind Nine, eds. S. R. Habbal et al. (The American Institute of Physics/Woodbury, NY), p.115
Srivastava N., Schwenn R., Inhester B., Martin S. F., Hanaoka Y., 2000, ApJ, 534, 468
St. Cyr O. C., Webb D. F., 1991, Solar Phys., 136, 379
Strauss H. R., 1986, Phys. Fluid, 29, 3668
Strauss H. R., 1988, ApJ, 326, 412
Sturrock P. A., 1980, in Solar flares: A monograph from Skylab Solar Workshop II, edited by P. A. Sturrock, Colorado Associated University Press, Boulder, Colo., p.411
Sturrock P. A., Weber M., Wheatland M. S., Wolfson R., 2001, ApJ, 380, 655
Sturrock P. A., 1991, ApJ, 380, 655
Sui L., Holman G. D., 2003, ApJ, 596, L251
Sui L., Holman G. D., Dennis B., 2004, ApJ, 612, 546
Sui L., Holman G. D., Dennis B. R., 2006, ApJ, 645, L157
Švestka Z., 1976, Solar Flares, Boston: D. Reidel
Švestka Z., 1981, in Solar Flare Magnetohydrodynamics, edited by E. R. Priest, Gordon and Breach Science Publishers, New York, p.47
Švestka Z., 1986, in The Lower Atmosphere of Solar Flares, ed. D. F. Neidig, NSO/SacPeak Publ., p.332
Švestka Z., 1995, Solar Phys., 160, 53
Švestka Z., 1996, Solar Phys., 169, 403
Švestka Z., Cliver E. W., 1992, in Eruptive Solar Flares, eds. Z. Švestka, B. V. Jackson, M. E. Machado, New York: Springer-Verlag, p.1
Švestka Z., Fontenla J. M., Machado M. E., Martin S. F., Neidig D. F., Poletto G., 1987, Solar Phys., 108, 237
Švestka Z., Fárník F., Hudson H. S., Hick P., 1998, Solar Phys., 182, 179
Švestka Z., Krieger A. S., Chase R. C., Howard R., 1977, Solar Phys., 52, 69
Tandberg-Hanssen E., 1974, Solar Prominences, Dordrecht: Reidel
Tang F., 1987, Solar Phys., 107, 233
Tang Y., Li Y., Fang C., Aulanier G., Schmieder B., Démoulin P., Sakurai T., 2000, ApJ, 534, 482
Tsuneta S., 1996, ApJ, 456, L63
van Ballegooijen A. A., Cartledge N. P., Priest E. R., 1998, ApJ, 501, 866
van Ballegooijen A. A., Martens P. C. H., 1989, ApJ, 343, 971

van Ballegooijen A. A., Priest E. R., MacKay D. H., 2000, ApJ, 539, 983
van Hoven G. et al., 1980, in Solar Flares: A Monograph from Skylab Solar Workshop II, edited by P. A. Sturrock, Colorado Associated University Press, Boulder, Colo., p.17
Vorpahl J. A., 1973, Solar Phys., 28, 115
Vourlidas A., 2004, in Solar and Space Weather Radiophysics: Current Status and Future Developments, eds., D. E. Gary, C. U. Keller, Boston: Kluwer, p.233
Vršnak B., Sudar D., Ruzdjak D., 2005, A&A, 435, 1149
Vršnak B., Warmuth A., Temmer M., Veronig A., Magdalenić J., Hillaris A., Karlický M., 2006, A&A, 448, 739
Wagner W. J., 1984, Ann. Rev. Astron. Astrophys., 22, 267
Wang H., Qiu J., Jing J., Zhang H., 2003, ApJ, 593, 564
Wang J., Shi Z., Martin S. F., 1996, A&A, 316, 201
Wang J., Shi Z., Martin S. F., Livi S. H. B., 1988, Vistas Astron., 31, 79
Wang J., Zhou G., Wen Y., Zhang Y., Wang H.-N. et al., 2006, Chin. J. Astron. Astrophys. (ChJAA), 6, 247
Wang Y.-M., Nash A. G., Sheeley N. R. Jr., 1989, Science, 245, 712
Wang Y.-M., Sheeley N. R. Jr., 1999, J. Geophys. Res., 510, L157
Webb D. F., Lepping R. P., Burlaga L. F., DeForest C. E., Larson D. E. et al., 2000, J. Geophys. Res., 105(A12), 27251
Webb D. F., Burkepile J., Forbes T. G., Riley P., 2003, J. Geophys. Res., 108(A12), 1440
Yokoyama T., Akita K., Morimoto T., Inoue K., Newmark J. 2001, ApJ, 546, L69
Wood P., Neukirch T., 2005, Sol. Phys., 226, 73
Zhang J., Wang J., Deng Y., Wu D., 2001a, ApJ, 548, L99
Zhang J., Dere K. P., Howard R. A., Kundu M. R., White S. M., 2001b, ApJ, 559, 452
Zhang M., Golub L., DeLuca E., Burkepile J., 2002, ApJ, 574, L97
Zhang Y., Hu Y., Wang J., 2005, ApJ, 626, 1096
Zhang Y., Wang J., Hu Y., 2006, ApJ, 641, 572
Zirin H., 1988, Book-Review − Astrophysics of the Sun, Cambridge University Press, New York
Zlotnik E. Y., Klassen A., Klein K.-L., Aurass H., Mann G., 1998, A&A, 331, 1087